J. Astron. Space Sci. 11(2), 250–272 (1994)

# THEORY AND SIMULATION OF BROADBAND ELECTROSTATIC NOISE IN THE MAGNETOTAIL

**S. Y. Kim**
Department of Physics
Korea Advanced Institute of Science and Technology,
Taejon 305-701, Korea

*(Received October 20, 1993; Accepted December 8, 1993)*

## ABSTRACT

Various plasma instabilities driven by the ion beams have been proposed in order to explain the broadband electrostatic noise (BEN) in the earth's geomagnetic tail. Ion acoustic, ion-ion two stream, and electron acoustic instabilities have been proposed. Here we consider a theoretical investigation of the generation of BEN by cold streaming ion beams in the earth's magnetotail. Linear theory analysis and particle simulation studies for the plasma sheet, which consists of warm electrons and ions as well as cold streaming ion beams, have been done. Both beam-ion acoustic and ion-ion two stream instabilities easily occur when the beam and warm electron temperature ratio, $T_b/T_e$ is small enough. The numerical simulation results confirm the existence of broadband electrostatic noise whose frequency is ranged from $\omega = 0$ to $\omega \sim \omega_{pe}$.

## 1. INTRODUCTION

The most frequent and intense broadband electrostatic noise (BEN), whose frequency band is from 10 Hz to 10 kHz (local plasma frequency), has been observed in the boundary layer region of the earth's magnetosphere. These electrostatic waves were observed in the geomagnetic tail at radial distances $R \sim 30 - 40R_E$, where $R_E$ is the earth's radius. A first observation of BEN was made by IMP 7 satellite (Scarf *et al.* 1974).

Later and more detailed study of BEN by IMP 8 satellite shows that the electric field intensity can vary from 50 $\mu V/m$ to 5 $mV/m$ and extends over a broad range of frequency from about 10 Hz to several kHz (Gurnett *et al.* 1976). They also noted

that the BEN occurs predominantly near the boundary layer of the neutral plasma sheet.

Shortly after these observation in the geomagnetic tail, the BEN was alse observed in the auroral zone (Gurnett and Frank 1977), whose frequency ranges from 5 Hz to 2 kHz, with peak intensity at 10 – 50 Hz. The BEN is most intense during an active aurora and may be associated with electromagnetic auroral hiss.

From the particles data of IMP 8, it was found that the BEN was associated with anisotropic ions streaming either sunward or antisunward. The anisotropies in the ion velocity distribution were observed near the boundary layer of the plasma sheet. These single beams, either earthward or tailward, observed in the plasma sheet boundary layer have an order of several keV energies (Decoster and Frank 1979, Eastman *et al.* 1984). These particles were accelerated in the region of 40-50 $R_E$ away from the earth. This acceleration mechanism is not yet identified. Along with single ion beams either tailward or earthward, two counter-streaming ion beams possibly due to distant tail acceleration are observed (Williams 1981, Eastman *et al.* 1984). In addition to KeV ion beams, Sharp *et al.* (1981) observed colder ion beams at tens or hundreds of eV streaming tailward due to an ionospheric source through double layer. The composition of the cold streaming ions is primarily $H^+$ and $O^+$ which are of ionospheric origin. It was suggested that the BEN is generated by currents or possibly energetic ions observed in that region.

In order to explain the generation of BEN in the geomagnetic tail, several theoretical investigations have been made. Ashour-Abdalla and Thorne (1978) consider two free energy sources, ion loss cone distribution and field aligned currents, to explain the BEN observed on auroral field lines. Huba *et al.* (1978) proposed that large plasma density and magnetic field gradients, and the presence of a cross field current carried by drifting ions cause the coupling between a lower hybrid wave and a drift wave. The growth rate of lower hybrid drift instability is peaked at near the lower hybrid frequency $\omega_{LH}$. However, this cannot explain the less frequent existence of BEN in the lobes or the central plasma sheet, because this theory requires very large density and magnetic field gradient to drive the instability.

Recently, Grabbe and Eastman (1984) propose an extensive analytic theory of ion beam instabilities in the plasma sheet boundary waves can be driven with frequencies from 0.001 $\omega_{pe}$ up to $\omega_{pe}$ when the ion beams are cold enough.

The work of Grabbe and Eastman (1984) stimulates several further theoretical researches in BEN. Omidi (1985) treats all the possible angles of wave propagation in the dispersion relation correctly, because the results of Grabbe and Eastman (1984) were based on the parallel propagation while observation indicated otherwise. Omidi

(1985) solves a modified dispersion relation numerically and shows that obliquely propagating waves have more growth rate than parallel propagation waves.

Dusenbery and Lyons (1985) argue that Grabbe and Eastman's analysis did not explain the association of intense broadband electrostatic noise with the warm ion beams in the boundary layer. Therefore, they try to study the wave generation including both cold and warm ion beams in their model. They found that their results basically agree with Grabbe and Eastman's result. When beam temperature is sufficiently warm, the waves can not be generated. However, when both the warm and cold ion beams are simultaneously present, the wave growth rates will be enhanced.

The theoretical attempts mentioned above were limited to linear theory. However, in the presence of large amplitude of waves, nonlinear effects should be taken into account. In order to understand the effect of the waves on the particle distribution, several simulation studies have been carried out. Ashour-Abdalla and Okuda (1986) introduce counter-streaming ion beams to generate beam ion acoustic, ion-ion two stream, and electrostatic ion cyclotron instability as possible candidates to explain the BEN, and investigate nonlinear evolution of the particle distributions in their simulation models. However, in their simulation study the ion beam drift speed was chosen very large. Here in this work, we consider a simulation study of BEN in the geomagnetic tail using more realistic plasma parameters and low drift speed of ion beams. Recently, Ashour-Abdalla and Okuda (1986) include cold electron species to excite the electron acoustic instability in the geomagnetic tail.

The paper is organized as follows. A linear theory of the BEN driven by cold streaming ion beams is briefly described in section 2. We present the simulation results for a plasma, consisting of hot plasma sheet ions and electrons, and cold ion beams in section 3. Finally, we summarize our results and conclude in section 4.

## 2. LINEAR THEORY

First we consider a situation in which the streaming, cold, ionospheric ion beams interact with warm electrons and ions in the boundary layer of the neutral plasma sheet. These ion beams are supposed to have been accelerated at the auroral zone by double layers, and stream through the plasma sheet. It is possible that the the beam ions are accelerated in the deep tail region. Both ions and electrons in the plasma sheet are assumed to have an isotropic Maxwellian distribution with temperature $T_i$ and $T_e$, respectively, while ionosperic ion beams are drifting Maxwellian along a given magnetic field with temperature $T_b$ and the drift speed $\pm v$. Furthermore, we assume that $T_e \gg T_b$ and $v \gg C_s$, where $C_s$ is the ion sound speed, so that

beam ion acoustic and ion-ion two stream inatability can be unstable. In the case of magnetized electrons and unmagnetized ions, the dispersion relation of electrostatic waves in the presence of background Maxwellian ions and electrons, as well as two counter-streaming Maxwellian ion beams, is given by (Omidi 1985)

$$1 + \frac{1}{k^2\lambda_e^2}\left[1+\frac{\omega}{\sqrt{2}kv_e\cos\theta}\exp(-\frac{k^2v_e^2\sin^2\theta}{\Omega_e^2})\sum_{n=-\infty}^{\infty}Z(\frac{\omega+m\Omega_e}{\sqrt{2}kv_e\cos\theta})I_m(\frac{k^2v_e^2\sin^2\theta}{\Omega_e^2})\right] + \frac{1}{k^2\lambda_i^2}\left[1+\frac{\omega}{\sqrt{2}kv_i}Z(\frac{\omega}{\sqrt{2}kv_i})\right] + \frac{1}{k^2\lambda_b^2}\left[2+\frac{\omega-kv\cos\theta}{\sqrt{2}kv_b}Z(\frac{\omega-kv\cos\theta}{\sqrt{2}kv_b})+\frac{\omega+kv\cos\theta}{\sqrt{2}kv_b}Z(\frac{\omega+kv\cos\theta}{\sqrt{2}kv_b})\right]=0 \quad (1)$$

where $\omega$, $k$, $v_e, v_i$, $v_b$, $v$, $\Omega_e$, $\lambda_e$, $\lambda_i$, $\lambda_b$, $Z$ and $I_m$ are the complex frequency, wave number, background electron thermal speed, background ion thermal speed, ion beam thermal speed, ion beam drift speed, electron gyrofrequency, background electron Debye length, background ion Debye length, ion beam Debye length, plasma dispersion function, and modified Bessel function of order m, respectively. Here, the model velocity distributions for plasma sheet ions and electrons can be taken as

$$f_i(\vec{v}) = \frac{n_i}{(2\pi T_i/m_i)^{3/2}}\exp(\frac{m_iv^2}{2T_i}) \quad (2)$$

and

$$f_e(\vec{v}) = \frac{n_e}{(2\pi T_e/m_e)^{3/2}}\exp(-\frac{m_ev^2}{2T_e}) \quad (3)$$

while the velocity distribution for the ion beams is taken to be

$$f_b(\vec{v}) = \frac{1}{2}\frac{n_b}{(2\pi T_b/m_i)^{3/2}}\left[\exp(-\frac{m_i(v-u)^2}{2T_b})+\exp(-\frac{m_i(v+u)^2}{2T_b})\right] \quad (4)$$

where $u$ is the drift speed along the magnetic field. The counter-streaming ion beams are symmetric with respect to the background plasma particles. Energetic beams trapped in the earth mirror field or ion beams generated at conjugate points at high latitudes cause the symmetry of these ion beams (Williams 1981).

The proper plasma parameters for plasma sheet boundary layer are following; the background electron temperature $T_e \sim 200 - 500eV$, the ion temperature $T_i \sim 50 - 100eV$, and ion beam energy 40 keV. In present analysis we assume $T_e/T_i = 4$, $T_i/T_b = 25$, $\Omega_e/\omega_{pe} = 1/2$, and $n_b/n_e = 2/3$. In order to see the effect of ion beam velocity or propagation angle of wave on ion beam instability, we try to vary both propagation angle and drift speed of ion beams.

When drift speed of ion beams does not exceed the electron thermal speed, ion acoustic instability or ion-ion two stream instability can be generated (Stringer 1964, Forslund and Shonk 1970). When $u > C_s \equiv (T_e/m_i)^{1/2}$, beam ion acoustic waves become unstable from electron inverse Landau damping. The frequency of the ion acoustic wave in the beam ion frame is given by $\omega = kC_s(n_b/n_e)^{1/2}$. This instability is discussed by Grabbe and Eastman (1984) and Dusenbery and Lyons (1985).

When the drift speed of the ion beam is less than the ion acoustic speed, $n < c_s$, but more than the ion beam thermal speed, $u > v_b$, ion-ion instability can be unstable if $T_e \gg T_b$ is satisfied (Stringer 1964, Forslund and Shonk 1970).

In order to find the solutions of Eq. (1) numerically, the Muller method has been used. For the electrons the terms from m $= -5$ to m $= 5$ have been kept, since the contribution of higher order terms is very small. Three different angles, 0°, 30°, and 60°, and three different drift speeds, $v/v_i = 0.5$ (smaller than ion acoustic speed), 6 (near ion acoustic speed), and 20 (well above ion acoustic speed) are used in the numerical computation of Eq. (1).

Fig. 1 indicates the real frequency and growth rate of ion beam driven electrostatic instability with respect to $k\lambda_e$ for $v/v_i = 0.5$. Clearly the existence of ion-ion instability with zero frequency from the symmetric ion beams with small drift speed is shown. The growth rate at the parallel propagation is larger in the entire region of $k\lambda_e$ than that at the oblique propagation. As $k\lambda_e$ increases, the growth rates increase. This growth rate due to ion-ion instability is typically larger than that due to ion acoustic instability. The ion-ion mode dominantly appears at very short wavelength $k\lambda_e \geq 1$, so that the hot electrons act as a neutralizing background. Since the ion-ion instability is a purely growing mode and its growth rate is much larger than the growth rate of ion acoustic wave, the dc electric field fluctuations can influence the population of plasma sheet ion, which is rest in the laboratory frame, substantially.

Fig. 2 indicates the real frequency and growth rate of ion beam driven electrostatic instability with respect to $k\lambda_e$ for $v/v_i = 6$. Since the ion beam drift speed is little larger than ion acoustic speed for these plasma parameters, beam ion acoustic wave is generated. The real frequency $\omega$ is shown as $\pm(kC_s(n_b/n_e)^{1/2} - kv\cos\theta)$

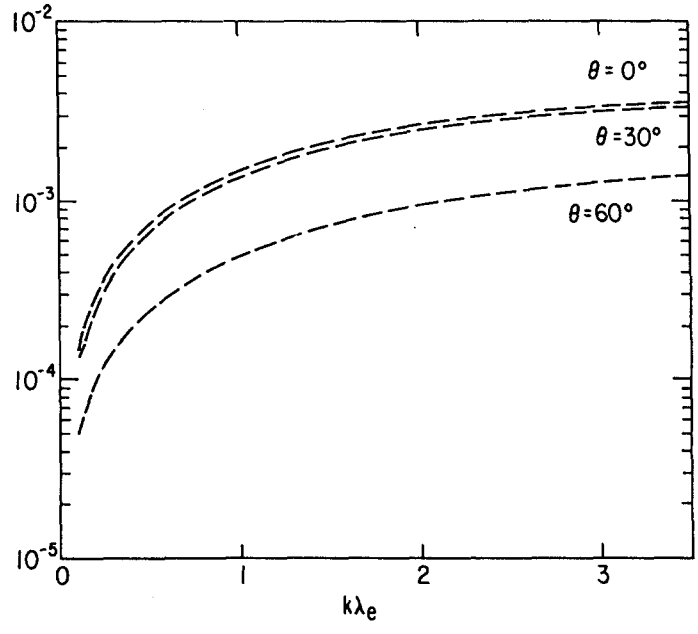


Figure 1. The growth rate (dotted curve) of counter-streaming ion beam driven electrostatic instability with respect to $k\lambda_e$ and propagation angle $\theta$ for $v/v_i = 0.5$. Here $T_e/T_i = 4$ and $T_i/T_b = 25$.

because of the symmetry of ion beam. This instability occurs because in the ion beam rest frame electron is drifting with velocity $v$ and this drifting electron can cause ion acoustic instability on beam ion via inverse Landau damping of electron. As the propagation angle $\theta$ becomes larger, Doppler effect is smaller thereby reducing real frequency. The growth rates at $\theta = 0°$ and $30°$ increase as $k\lambda_e$ increases. However, the growth rate at $\theta = 60°$ is peaked at about $k\lambda_e \sim 1$ and decreases as $k\lambda_e$ increases further. This is due to the fact that the phase velocity $\omega/k_\parallel$ is located where the gradient of electron velocity distribution is maximum so that growth rate is maximized at $k\lambda_e < 1$ for $\theta = 60°$.

Fig. 3 shows the real frequency and growth rate of ion beam driven instability with respect to $k\lambda_e$ for $v/v_i = 20$. As is expected from the beam drift speed well above ion acoustic speed, beam ion acoustic wave is generated.

As the propagation angle $\theta$ becomes larger, the real frequency becomes smaller as expected from Doppler effect. The growth rates at different angles of propagation

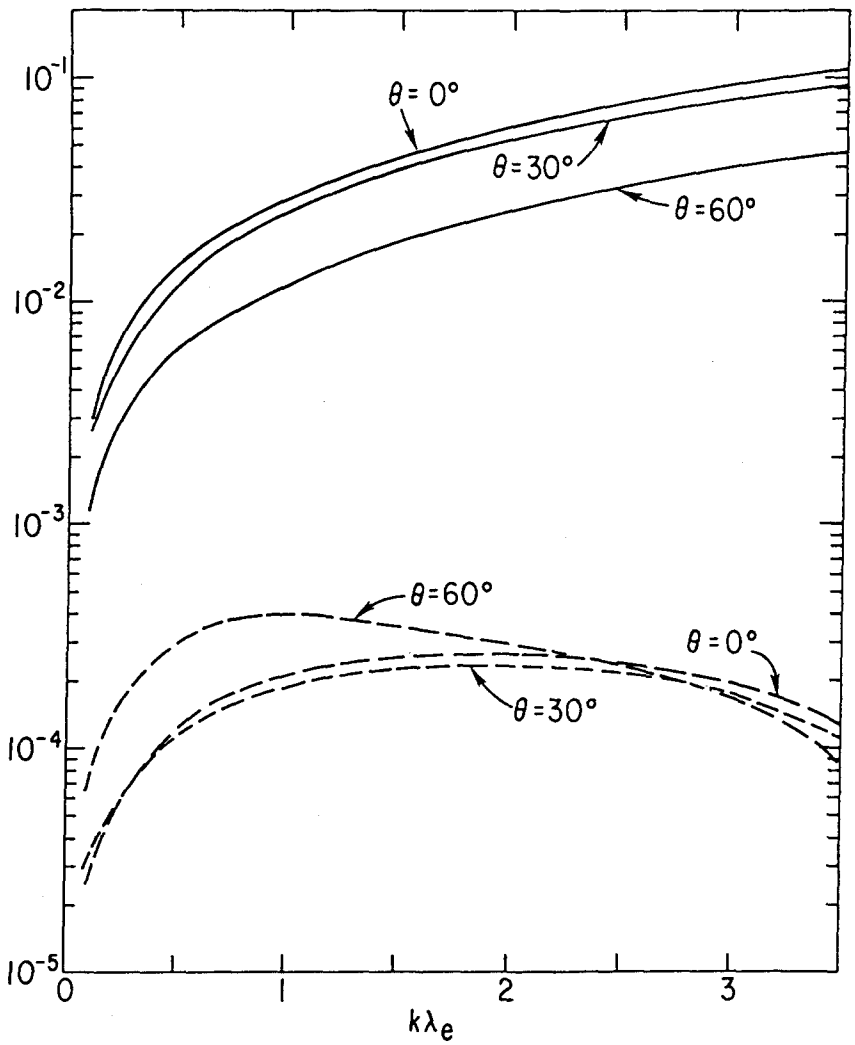


Figure 2. The real frequency (solid curve) and growth rate (dotted curve) of counter-streaming ion beam driven electrostatic instability with respect to $k\lambda_e$ and popagation angle $\theta$ for $v/v_i = 6$. Here $T_e/T_i = 4$ and $T_i/T_b = 25$.

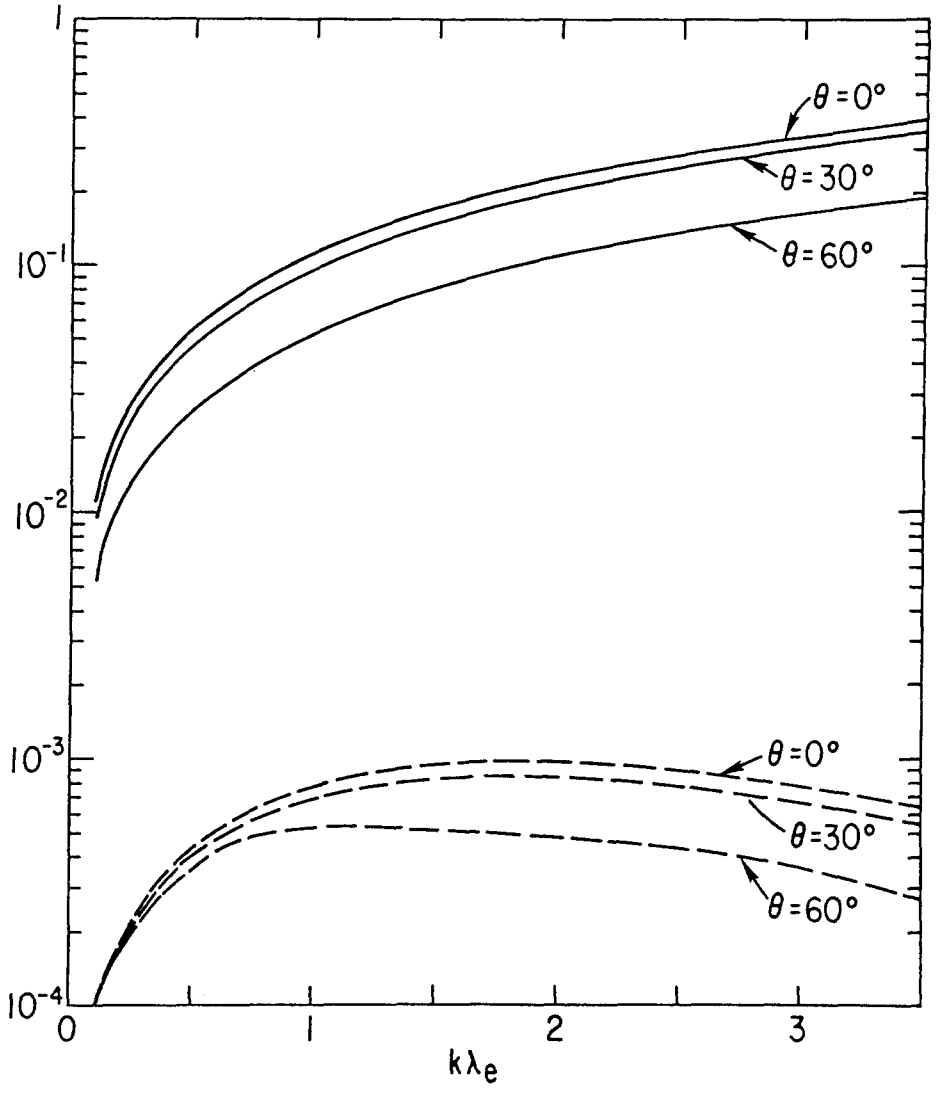


Figure 3. The real frequency (solid curve) and growth rate (dotted curve) of counter-streaming ion beam driven electrostatic instability with respect to $k\lambda_e$ and propagation angle $\theta$ for $v/v_i = 20$. Here $T_i/T_b = 25$.

are peaked near at $k\lambda_e \geq 1$ and decrease as $k\lambda_e$ increases further. As a comparative study of both counter-streaming and single ion beam driven electrostatic instability, we try to consider a single cold ionospheric ion beam driven electrostatic instability. In Eq. (1), we take only one single ion beam and recalculate the dispersion relation for different angles of propagation of wave. The plasma parameters we used here are very similar to the previous case, $T_e/T_i = 4$, $T_i/T_b = 25$, and $v/v_i = 5$. The same method has been used to obtain the solutions of dispersion relation.

Fig. 4 indicates the real frequency and growth rate of ion beam driven instability with respect to $k\lambda_e$ for $v/v_i = 5$. Since the drift speed is larger than ion acoustic speed for these parameters, beam ion acoustic wave is generated. The real frequency and growth rate in this case are very similar to those obtained in Fig. 2. The difference between counter-streaming and single ion beam case is that there are two resonant points, $v = \pm\omega/k_\parallel$ where beam ion acoustic wave is unstable, in the case of counter-streaming ion beam driven instability. However, there is only one resonant point where beam ion acoustic mode is unstable for the single beam driven instability. The growth rate for beam ion acoustic wave is enhanced in the case of the single ion beam driven electrostatic instability since beam density is a little bit larger than the counter-streaming ion beam case.

## 3. SIMULATION

In order to study the BEN and its associated particle distributions, we consider a two-dimensional electrostatic particle simulation in the presence of background ions and electrons as well as counter-streaming ion beams along the magnetic field. It is important to use a two-dimensional mode here so that many modes with different wave numbers, angles of propagation, and frequencies become excited at the same time generating the BEN.

The simulation model used here is a 2-1/2 dimensional electrostatic simulation model - two coordinate space (x, y) and three velocity space ($v_x$, $v_y$, $v_z$) in a uniform magnetic field $\vec{B}_0$ which lies in the y-z plane $\vec{B} = (0, B_y, B_z)$. We use full dynamics for the motion of ions and electrons. The simulation parameters used here are $\Omega_e/\omega_{pe} = 0.5$, $\lambda_e = \Delta$, and $m_i/m_e = 1836$, where $\Omega_e$, $\omega_{pe}$, $\lambda_e$ and $\Delta$ are electron gyrofrequency, electron plasma frequency, electron Debye length, and grid size, respectively. Typically, a $64 \times 64$ grid has been used with 9 particles per unit cell. The other simulation parameters are following: $T_i/T_b = 25$, $T_e/T_i = 4$, $B_y/B_o = 0.866$, $n_{b+} = n_{b-} = n_i = n_e/3$, where $n_{b\pm}$, $n_i$ and $n_e$ are ion beam density, plasma sheet ion density, plasma sheet electron density, respectively.

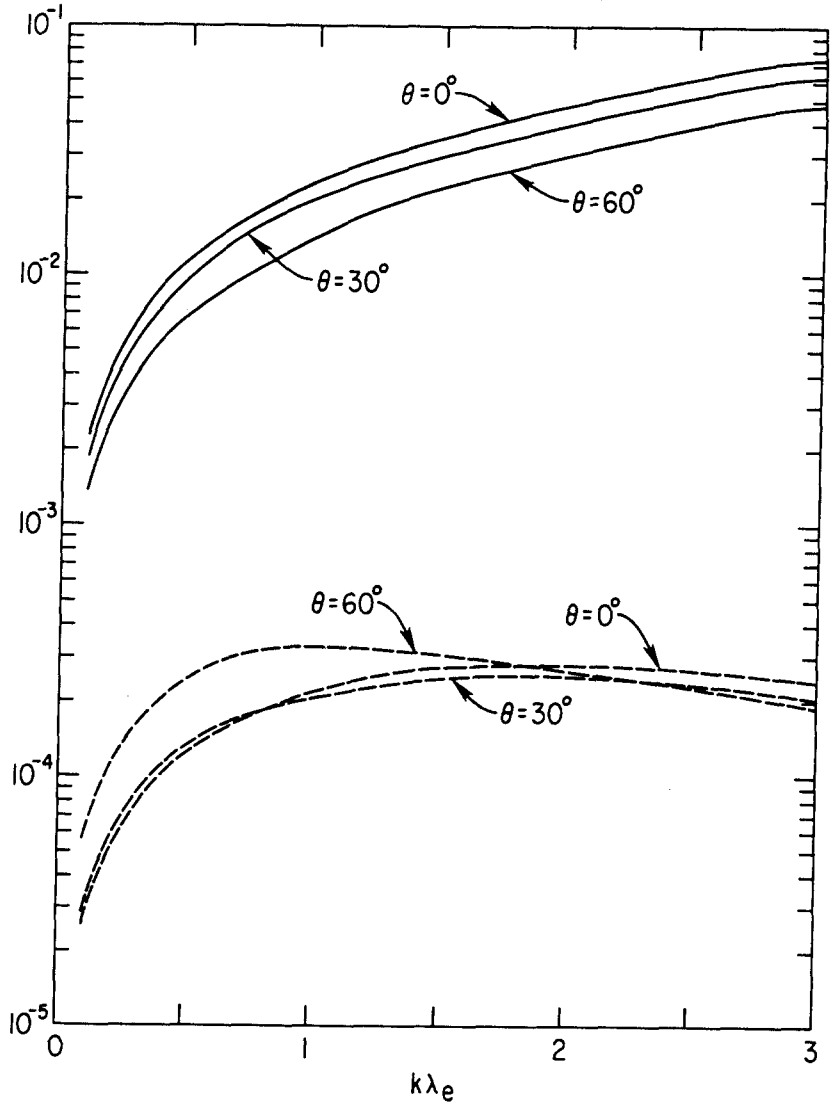


Figure 4. The real frequency (solid curve) and growth rate (dotted curve) of single ion beam driven electrostatic instability with respect to $k\lambda_e$ and propagation angle $\theta$ for $v/v_i = 5$. Here $T_e/T_i = 4$ and $T_i/T_b = 25$.

The first example considered here is a situation where counter-streaming ion beams interact with warm plasma electrons and ions in the neutral plasma sheet. The ion beams are drifting with speed $v = \pm 4v_i$ where $v_i$ is the thermal speed of warm ions. Such simulation parameters are determined since cold ionospheric ions at 1 eV are accelerated to 10 KeV drift kinetic energy by the electric field of double layer through a $100 \sim 200eV$ plasma at the neutral sheet boundary layer.

The external magnetic field is taken in the y-z plane, $\vec{B} = (0,\ B_y,\ B_z)$, so that the waves in the simulation model are obliquely propagating. In the presence of cold ion beams a number of electrostatic waves can be excited. Ion acoustic waves on the beam ions can be unstable by warm electrons for both parallel and oblique propagations with respect to the external magnetic field. Electrostatic ion cyclotron waves can also be excited either by electron or ion beams. They predominantly propagate across the magnetic field.

Fig. 5 shows the electron and ion velocity distributions at $t = 0$ (initial) and $t = 3240\omega_{pe}^{-1}$. Fig. 5 (a), (b), and (c) indicate electron two perpendicular and parallel velocity distributions with respect to the magnetic field, respectively. These results show a small amount of electron heating occurs by obliquely propagating beam ion acoustic wave and ion-ion instability. Fig. 5(d), (e), and (f) show both background and beam ion two perpendicular and parallel velocity distributions, which indicate that both ion acoustic wave and ion-ion instability heat both beam and background ion in the parallel and perpendicular direction.

In order to observe the different rate of heating for both background and beam ions, we separately plot the velocity distributions of two different ions in Fig. 6 (a), (b) and (c) which show ion beam two perpendicular and parallel velocity distribution, respectively. Fig. 6 (d), (e), and (f) indicate background ion two perpendicular and parallel velocity distributions, respectively. The remarkable heating of ion beam occurs in both parallel and perpendicular direction with respect to the magnetic field. On the other hand the substantial heating of background ion parallel velocity occurs due to dc ion-ion instability and little effect of background ion perpendicular heating is observed.

In order to confirm the existence of beam ion acoustic wave and ion-ion instability, we shall now study the frequency spectrum of eletric field for different Fourier modes. Fig. 7 (a) and (b) show the time history and the power spectrum of the (2,2) mode propagating obliquely across the magnetic field with $\theta \sim 52°$, where $k_x \sim 0.2$ and $k_y \sim 0.2$, respectively. In Fig. 7 (a) a slowly growing low frequency instability is seen whose frequency spectrum is shown in Fig. 7 (b). There are two large peaks near $\omega \sim \pm[kc_s(n_b/n_e)^{1/2} - kv\cos\theta]$, which are ion acoustic waves of the beam ion

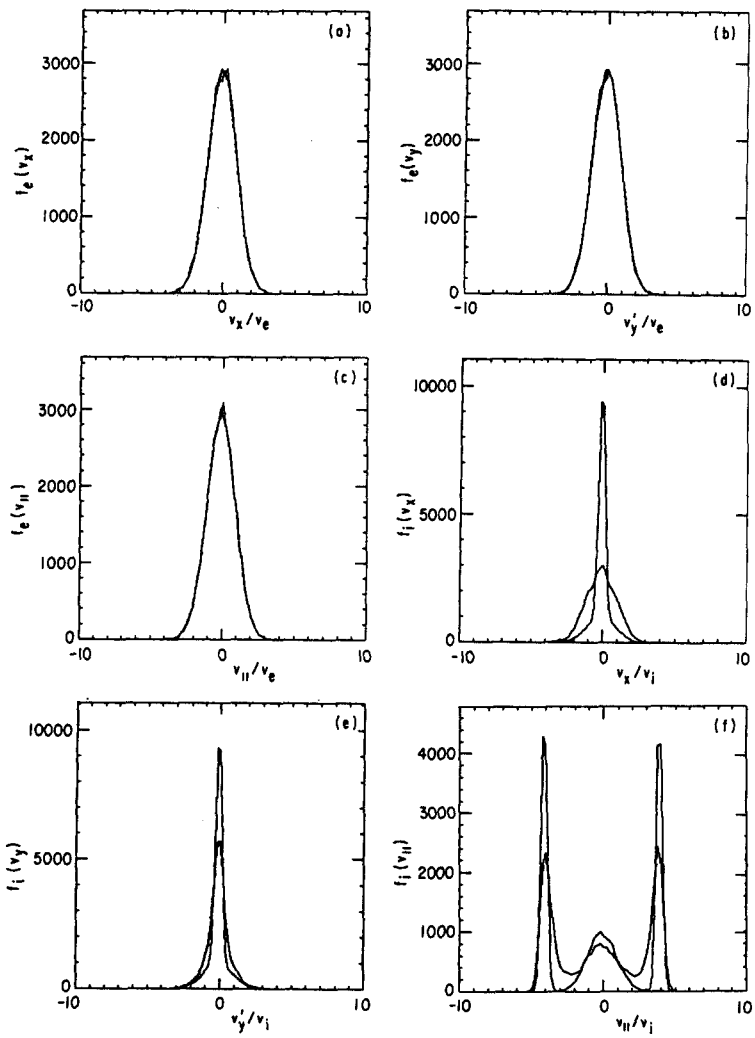


Figure 5. Two components of electron perpendicular velocity distribution at initial and final time (a), (b). Electron velocity distribution along the magnetic field at initial and final time (c). Two components of background and beam ion velocity distribution along the magnetic field at initial and final time (f).

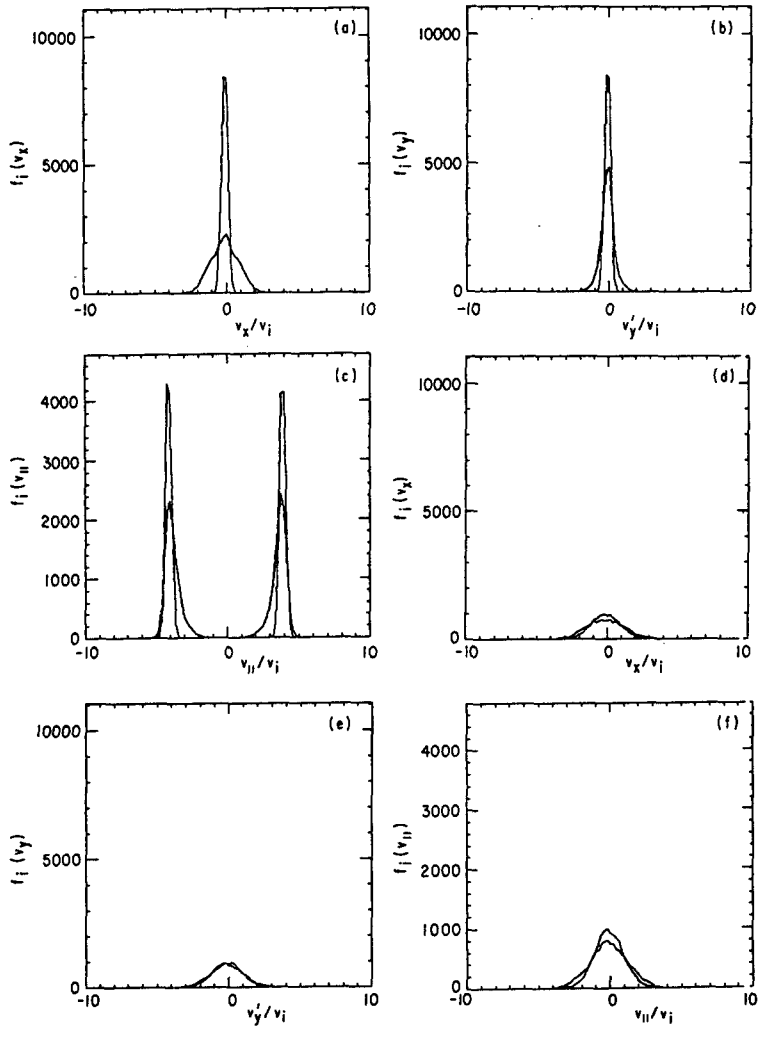


Figure 6. Two components of electron perpendicular velocity distribution at initial and final time (a), (b). Beam ion velocity distribution along the magnetic field at initial and final time (c). Two components of background ion perpendicular velocity distribution at initial and final time (d), (e). Background ion velocity distribution along the magnetic field at initial and final time (f).

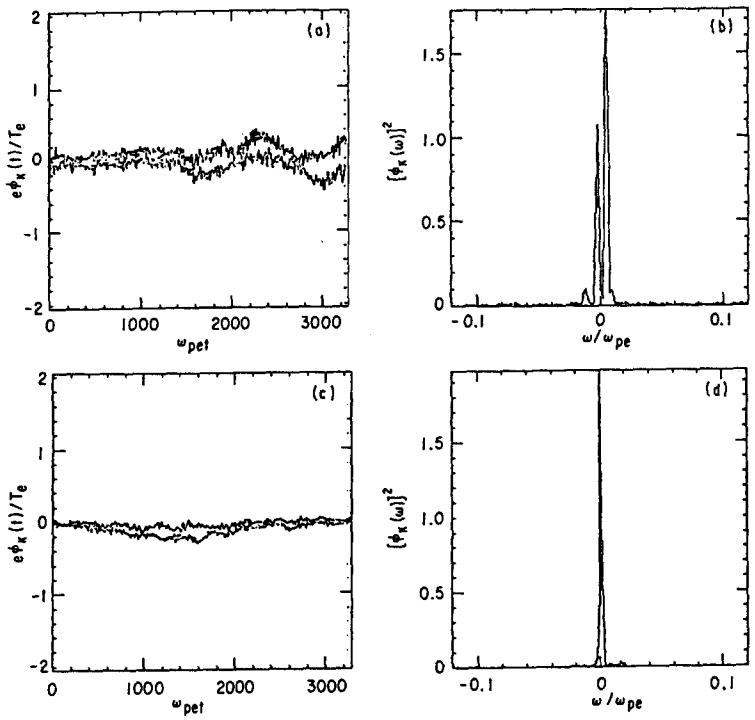


Figure 7. Time history of Fourier mode (2, 2) (a) and its power spectrum (b). Time history of Fourier mode (6, 2) (c) and its power spectrum (d).

observed in a laboratory frame. Fig. 7 (c) and (d) show the time history and power spectrum for the (6,2) mode propagating more obliquely across the magnetic field with $\theta \sim 72°$ where $k_x \sim 0.6$ and $k_y \sim 0.2$ respectively. Since the effective ion beam drift speed of, in the direction of wave vector, $v(k_\parallel/k)$ becomes smaller, zero frequency ion-ion instability rather than ion acoustic wave is observed. This mode is responsible for the heating of ion in the neutral plasma sheet.

The power spectrum for the individual Fourier mode shows the presence of coherent peaks, and the broadband nature of the electrostatic instability up to $\omega \sim \omega_{pe}$ can be obtained when we sum over all the wavelength modes in the simulation data (Ashour-Abdalla and Okuda, 1986).

The second example is a situation where counter-streaming ion beams interact

with warm plasma ions and electrons in the neutral sheet with a drift speed of $v = \pm 25 v_i$. The simulation parameters used here are the same as those of first case except the drift speed mentioned above.

Fig. 8 shows that the electron and ion velocity distributions at $t = 0$ (initial) and $t = 3240\omega_{pe}^{-1}$. Fig. 8 (a), (b), and (c) indicate electron two perpendicular and parallel velocity distribution with respect to the magnetic field, respectively. These results show a small amount of electron heating occurs by obliquely propagting beam ion acoustic wave. Fig. 8 (d), (e), and (f) show background ion velocity distribution and Fig. 8 (g), (h), and (i) show beam ion two perpendicular and parallel velocity distribution with respect to the magnetic field. Very little heating of both background and beam ion is observed.

Fig. 9 shows the time history and frequency spectrum of two different Fourier modes propagating across the magnetic field. Fig. 9 (a) and (b) show the time history and power spectrum (5,1) mode with $\theta \sim 80°$, where $k_x \sim 0.5$ and $k_y \sim 0.1$, respectively. In both cases a slowly growing low frequency instability is observed due to beam ion acoustic instability.

The third example is a situation where counter-streaming ion beams are drifting with speed of $V = \pm 0.5 V_i$ to the boundary layer which consists of warm plasma ions and electrons. The simulation parameters used here are same as the first case except the ion beam drifting speed.

Fig. 10 shows both electron and ion velocity distributions at both $t = 0$ (initial) and $t = 3240\omega_{pe}^{-1}$. Fig. 10 (a) and (b) indicate electron perpendicular and parallel velocity distributions, respectively. These results show a very little heating of electron by obliquely propagating ion-ion instability. Fig. 10 (c) and (d) indicate beam ion perpendicular and parallel velocity distributions, and Fig. 10 (e) and (f) show background ion perpendicular and parallel velocity distribution. Ion beam perpendicular and parallel heating is rather substantial, while background ions do not experience too much.

Fig. 11 shows the time history and frequency spectrum of different Fourier modes. Fig. 11 (a) and (b) indicate both time history and frequency spectrum of obliquely propagating mode (0, 2) with $\theta \sim 30°$ where $k_x \sim 0$ and $k_y \sim 0.2$, respectively. Fig. 11 (c) and (d) indicate both time history and frequency spectrum of obliquely propagating mode (1, 3) with $\theta \sim 34°$ where $k_x \sim 0.1$ and $k_y \sim 0.3$, respectively. Clearly a slowly growing signal with zero frequency ion-ion instability is observed.

In order to compare the simulation results of electorstatic instability driven by both counter-streaming and single ion beam, we try to consider a simulation model which consists of neutral plasma sheets and single cold ionospheric ion beam from the

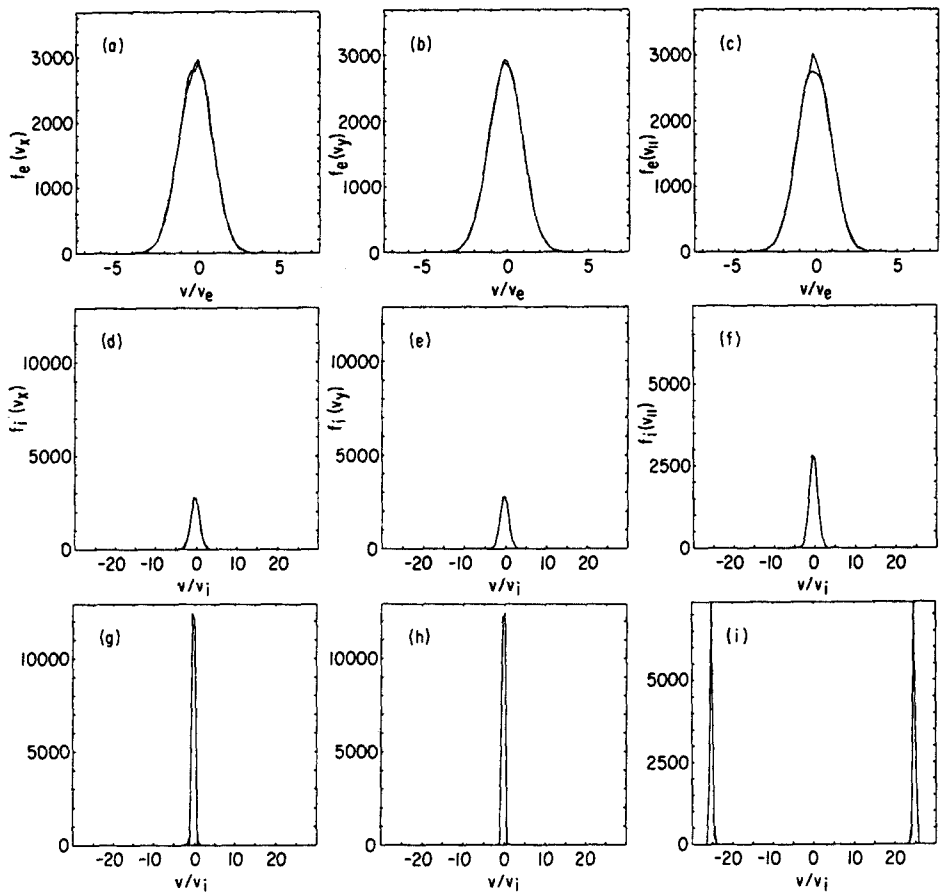


Figure 8. Two components of electron perpendicular velocity distribution at initial and final time (a), (b). Electron velocity distribution along the magnetic field at initial and final time (c). Two components of background ion perpendicular velocity distribution at initial and final time (d), (e). Background ion velocity distribution along the magnetic field at initial and final time (f). Two components of beam ion perpendicular velocity distribution at initial and final time (g), (h). Beam ion velocity distribution along the magnetic field at initial and final time (i).

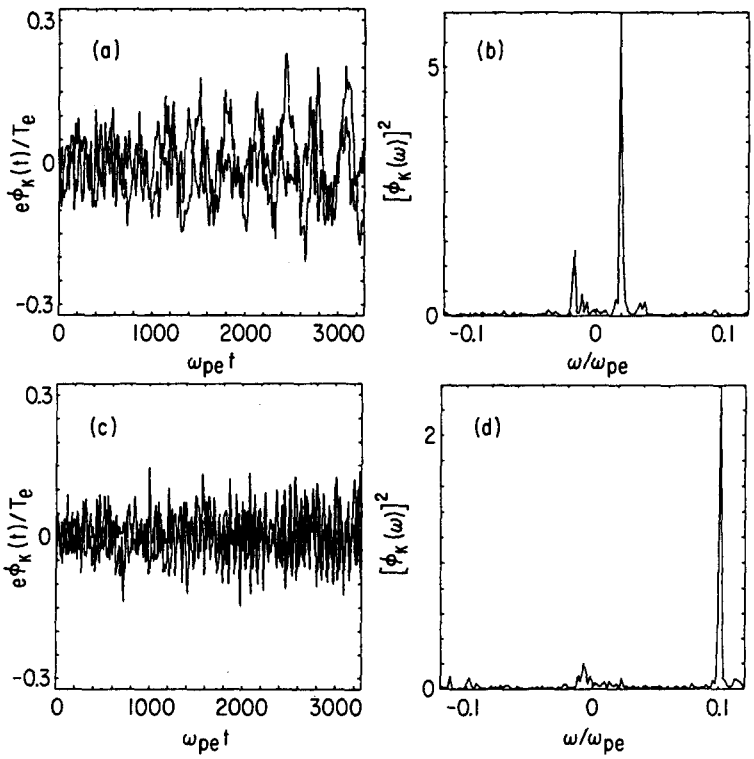


Figure 9. Time history of Fourier mode (5, 1) (a) and its power spectrum (b). Time history of Fourier mode (3, 4) (c) and its power spectrum (d).

ionosphere. We use 2-1/2 dimensional eletrostatic simulation model - two coordinate space (x, y) and three velocity space ($V_x$, $V$, $V_z$) in a uniform magnetic field $\vec{B_0}$ which lies in the y axis $\vec{B} = (0,\ B,\ 0)$. The simulation parameters are $\Omega_e/\omega_{pe} = 0.2$, $\lambda_e = \Delta$, and $m_i/m_e = 1836$. Full particle dynamics for the motion of both ions and electrons are used. The other parameters are following : $T_i/T_b = 25$, $T_e/T_i = 4$, $n_b = n_i = 1/2n_e$, $v/v_i = 5$, where $v$ is the ion beam drift speed.

Fig. 12 shows the electron and ion velocity distributions at $t = 0$ and $t = 3240\ \omega_{pe}^{-1}$. Fig. 12 (a) and (b) indicate electron perpendicular and parallel velocity distributions, respectively. These results show a small amount of electron heating occurs by obliquely propagating beam ion acoustic wave. Fig. 12 (c) and (d) show beam ion perpendicular and parallel velocity distributions. Beam ion acoustic wave

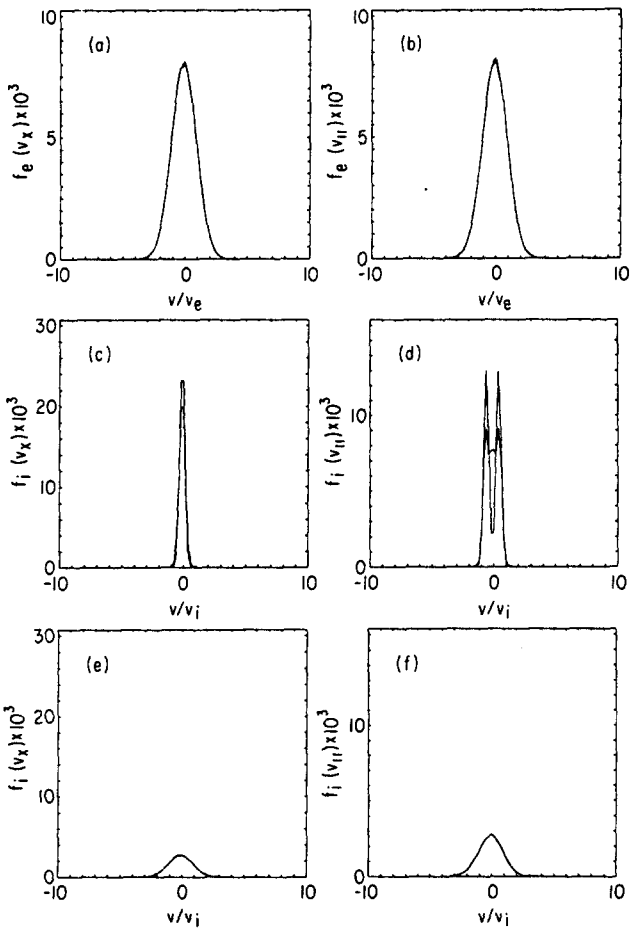


Figure 10. Electron perpendicular velocity distribution at initial and final time (a) Electron velocity distribution along the magnetic field at initial and final time (b) Beam ion perpendicular velocity distribution at initial and final time (c). Beam ion velocity distribution along the magnetic field at initial and final time (d). Background ion perpendicular velocity distribution at initial and final time (e). Background ion velocity distribution along the magnetic field at initial and final time (f).

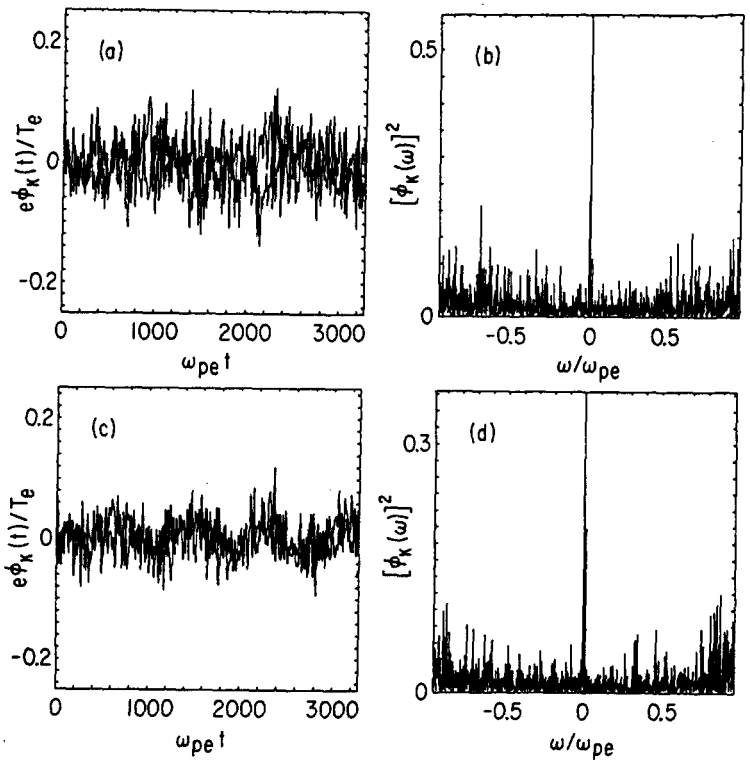


Figure 11. Time history of Fourier mode (0, 2) (a) and its power spectrum (b). Time history of Fourier mode (1, 3) (c) and its power spectrum (d).

heats ion beam perpendicular velocity in a symmetric manner as shown in Fig. 12 (c). Fig. 12 (e) and (f) show background ion perpendicular and parallel velocity distributions. The asymmetry of background ion parallel velocity heating is due to the single ion beam driven instability, where there is only one resonant point to make the wave unstable.

Fig. 13 shows the time history and frequency spectrum of different Fourier modes. Fig. 13 (a) and (b) indicate both time history and frequency spectrum of obliquely propagating mode (1, 2) with $\theta \sim 26°$ where $k_x \sim 0.1$ and $k_y \sim 0.2$, respectively. Fig. 13 (c) and (d) indicate both time history and frequency spectrum of obliquely propagating mode (4, 2) with $\theta \sim 63°$ where $k_x \sim 0.4$ and $k_y \sim 0.2$, respectively. Both cases show the clearly growing signal with beam ion acoustic wave frequency

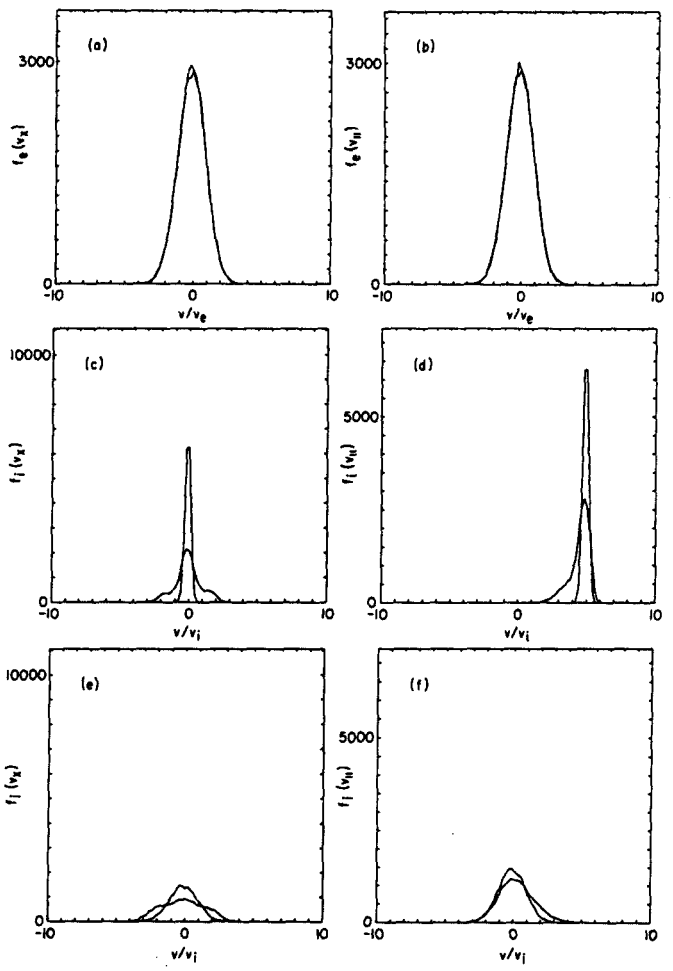


Figure 12. Electron perpendicular velocity distribution at initial and final time (a). Electron velocity distribution along the magnetic field at initial and final time (b). Beam ion perpendicular velocity distribution at initial and final time (c). Beam ion velocity distribution along the magnetic field at initial and final time (d). Background ion perpendicular velocity distribution at initial and final time (e). Background ion velocity distribution along the magnetic field at initial and final time (f).

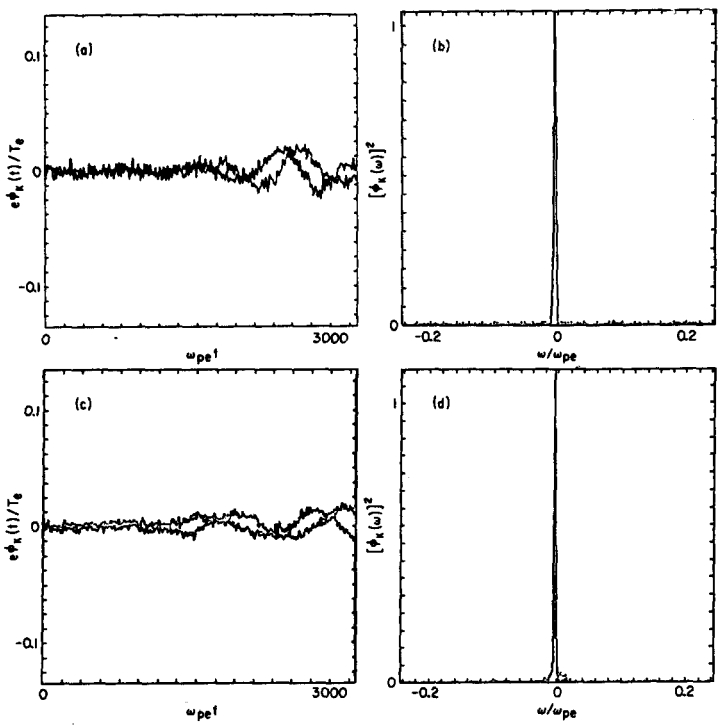


Figure 13. Time history of Fourier mode (1, 2) (a) and its power spectrum (b). Time history of Fourier mode (4, 2) (c) and its power spectrum (d).

agreed with theoretical values.

Fig. 14 also shows the time history and frequency spectrum of different Fourier modes. Fig. 14 (a) and (b) indicate both time history and frequency spectrum of obliquely propagating mode (3, 4) with $\theta \sim 37°$, respectively. Fig. 14 (c) and (d) indicate both time history and frequency spectrum of obliquely propagating mode (4, 4) with $\theta \sim 45°$, respectively. Fig. 14 (e) and (f) indicate both time history and frequency spectrum of obliquely propagating mode (5, 4) with $\theta \sim 51°$, respectively. When the angle of propagation is larger, the effective velocity $v_{\|} = v(k_{\|}/k)$ is smaller and real frequency becomes smaller, however the saturation levels are roughly same - which is due to the fact that growth rates of three modes are not so different. Clearly a slowly growing signal with beam acoustic wave frequency has also been observed.

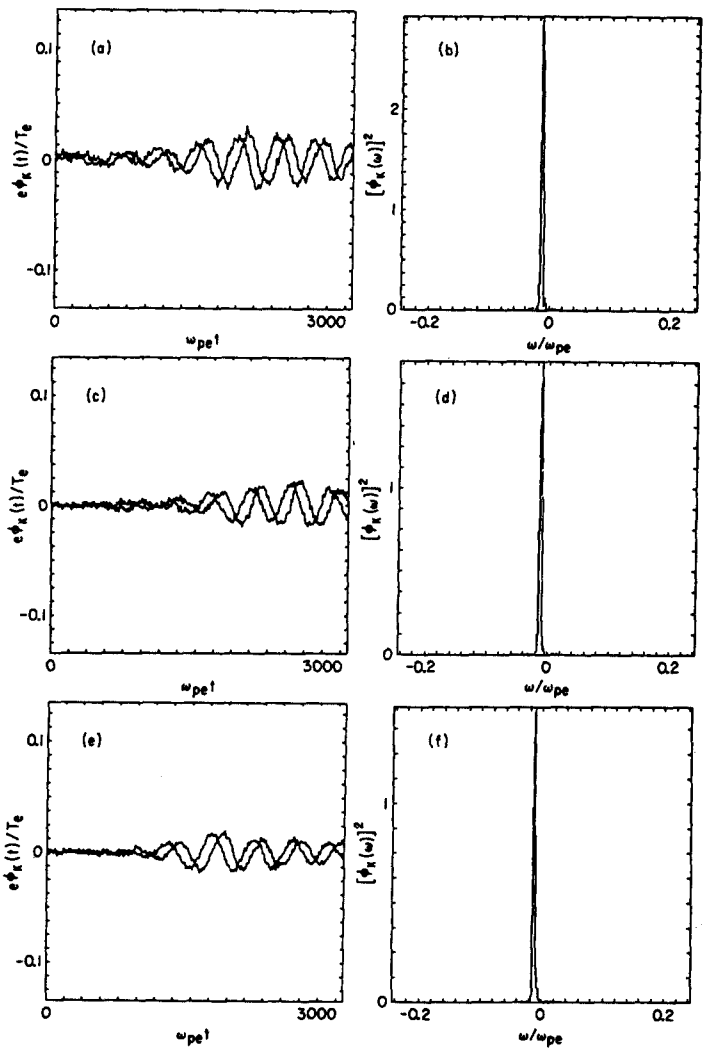


Figure 14. Time history of Fourier mode (3, 4) (a) and its power spectrum (b). Time history of Fourier mode (4, 4) (c) and its power spectrum (d). Time history of Fourier mode (5, 4) (e) and its power spectrum (f).

## 4. DISCUSSION AND CONCLUSION

Here we have shown the excitation of obliquely propagating ion acoustic instability and ion-ion instability due to both sigle and counter-streaming cold ion beams in the boundary layer of neutral sheet. Both cases indicate the similar aspects of generating BEN in the magnetotail. Even though the power spectra of each Fourier mode show a presence of sharp peaks, summation over the Fourier modes, which corresponds to a single point observation done by a satellite, reveals a broader spectrum whose frequency extends from $\omega \sim 0$ to $\omega \sim \omega_{pe}$. Beam ion acoustic instability is most likely responsible to the generation of broadband electrostatic noise, it causes only slight heating of beam and background ions themselves. However, the coexistence of ion acoustic and ion-ion instability gives rise to substantial heating of ions.

**ACKNOWLEDGEMENTS** : This work was supported by KAIST Basic Research Fund.

## REFERENCES

Ashour-Abdalla, M. & Thorne, R. M. 1978, J. Geophys. Res., 83, 4755
Ashour-Abdalla, M. & Okuda, H. 1986, J. Geophys. Res., 91, 6833
Ashour-Abdalla, M. & Okuda, H. 1986, Geophys. Res. Lett., 13, 366
Decoster, R. J. & Frank, L. A. 1979, J. Geophys. Res., 84, 5099
Dusenbery, P. B. & Lyons, L. R. 1985, J. Geophys. Res., 90, 10935
Eastman, T. E., Frank, L. A. & Peterson, W. 1984, J. Geophys. Res., 89, 1553
Forslund, D. W. & Shonk, C. R. 1970, Phys. Rev. Lett., 25, 281
Grabbe, C. L. & Eastman, T. E. 1984, J. Geophys. Res., 89, 3865
Gurnett, D. A., Frank, L. A. & Lepping, R. 1976, J. Geophys. Res., 81, 6059
Gurnett, D. A. & Frank, L. A. 1977, J. Geophys. Res., 82, 1031
Huba, J. D., Gladd, N. T. & Papadopoulos, K. 1978, J. Geophys. Res., 83, 5217
Omidi, N. 1985, J. Geophys. Res., 90, 12330
Scarf, F., Frank, L. A., Ackerson, K. L. & Lepping, R. 1974, Geophys. Res. Lett., 1, 189
Sharp, R. D., Carr, D. L., Peterson, W. K. & Shelly, E. G. 1981, J. Geophys. Res., 86, 4639
Stringer, T. E. 1964, Plasma Phys., 6, 267
Williams, D. 1981, J. Geophys. Res., 86, 5507